Macromolecular Materials and Engineering
Open Access
www.mame-journal.de

Surfactant-Modified Progesterone-Loaded PVP/Cellulose Fibres for Future Drug Delivery Applications in Menopause

*Omar Shafi, Michelle Swer, Un Hou Chan, Alisha Kassam, Mirkomol Mirzarakhimov, Jai Yi Huang, and F Brako**

Menopause often results in symptoms that impact physical and mental well-being, and hormone replacement therapy (HRT) using progesterone (PGS) is a common treatment. This study explores PGS-loaded transdermal cellulose-based binary fibres as a potential adjunct for oestrogen in HRT. Using ethyl cellulose (EC) and cellulose acetate (CA) bound with Polyvinylpyrrolidone (PVP), the release of PGS is studied via a Franz Diffusion Cell system. Various analyses, including rheology, SEM, FTIR, in vitro drug release, and mathematical modelling, are conducted. SEM revealed that CA fibres are thinner than EC fibres, and FTIR showed more uniform PGS distribution in CA fibres. In vitro drug release tests indicated 400–600 µg of PGS is released from 11.9 mg fibre patches into 5mL PBS within 70 min, demonstrating effective drug penetration. Adding Polysorbate 80 (PS80) significantly increased PGS release. The Makoid-Banakar model best suited EC fibres, while both the Makoid-Banakar and Peppas Sahlin models fit CA fibres. These findings suggest that the fibrous patches offer a convenient, minimally invasive, and personalised method for delivering precise PGS doses in HRT. The study sets a strong foundation for further in vivo and cytotoxicity testing to validate the clinical effectiveness and safety of these patches in alleviating menopausal symptoms.

1. Introduction

Menopause impacts ≈13 million women in the UK and ≈1 billion globally, with the average age ≈51.[1,2] It is characterised by the absence of menstruation due to the loss of ovarian follicular activity.[2,3] The transition leading up to menopause, known as perimenopause, can last up to five years and is marked by fluctuating hormone levels that contribute to early symptoms.[4] Premature ovarian failure or iatrogenic reasons, such as surgery or chemotherapy, can also induce early menopause. The symptoms include hot flushes, night sweats, and mood changes.[5] This significant life stage profoundly affects the well-being of women, impacting their overall quality of life. Managing menopausal symptoms can be achieved through HRT, involving the use of both oestrogen with PGS.[4,5] Women with contraindications to oestrogen need PGS in their management to prevent endometrial hyperplasia, while also benefiting from its role in alleviating vasomotor symptoms and providing mood stabilisation.[6–8] However, for those who specifically request dosage forms such as Oestrogel for its cooling effects, or oestrogen loaded sprays, alternative PGS forms are necessary to address this requirement.

This research embarks on a promising avenue, introducing a transdermal fibrous patch as a potentially novel approach to address the limitations of PGS delivery. Existing methods, such as oral ingestion and vaginal or rectal application, have their

O. Shafi, J. Y. Huang
Torrington Place
Department of Mechanical Engineering
University College London
London WC1E 6BT, UK

M. Swer
London Gynaecology
15 Austin Friars, London EC2N 2HE, UK

U. H. Chan
Department of Bioengineering
Imperial College London
London SW7 2AZ, UK

A. Kassam
UCL Medical School
74 Huntley Street, London WC1E 6DE, UK

M. Mirzarakhimov
Brunel Medical School
Uxbridge UB8 3PH, UK

F Brako
Faculty of Engineering and Science
University of Greenwich
Chatham, Kent ME4 4TB, UK
E-mail: f.brako@greenwich.ac.uk

The ORCID identification number(s) for the author(s) of this article can be found under https://doi.org/10.1002/mame.202500023

DOI: 10.1002/mame.202500023

drawbacks, including hepatic bypass metabolism, discomfort and loss of dignity during administration.[9] These limitations can hinder PGS accessibility and, in turn, reduce patient adherence.[10] In contrast, a patient-centred transdermal patch with longer-lasting transdermal drug delivery offers a promising solution.[7] The PGS patch stands out among new PGS therapy options, boasting advantages like a patient-friendly application process and avoidance of excessive hepatic metabolism seen in oral formulations.[6] Transdermal patches for hormone therapy have long been used to deliver oestrogen and combination treatments, typically placed on the abdomen, buttocks, upper outer arm, or thigh—sites chosen for their balance of drug permeability, adhesion stability, and discretion. Given these established practices, the fibrous PGS patch, enhanced with PS80 for improved permeability, would be optimally placed on the lower abdomen or upper buttocks, ensuring both effective drug absorption and user comfort while maintaining concealability (REF). Moreover, the track record of oestrogen transdermal patches containing PGS indicates no increased risk of venous thromboembolism, instilling confidence in patch delivery.[7,11,12] The PGS patch offers varied dosage options, enhancing therapy customisation for clinicians seeking independent endometrial protection. This flexibility allows tailored treatment plans, distinct from combined patches, tablets, capsules, or intrauterine devices. The patch is a strong complement, particularly appealing to those preferring standalone oestrogen in gel or spray forms. This research explores the innovative transdermal approach, advancing PGS therapy in the future.

Polymeric fibrous patches are gaining recognition as a promising tool for transdermal drug delivery. These patches possess adjustable characteristics, such as porosity, which aid in the diffusion and dissolution of drugs from their fibrous structure.[13,14] Once released from these fibres at a specified particle size (typically molecules with a molecular weight less than 400 kDa), the drug encounters the stratum corneum.[15,16] Through passive diffusion, it proceeds via intercellular pathways within the lipid matrix, advancing into the epidermis, and ultimately gaining access to capillaries for entry into the bloodstream.[16,17] A binary polymeric transdermal drug delivery system has been employed due to its strong affinity for active substances.[18–20] This study uses two cellulose derivatives, EC and CA, with PVP. Cellulose derivatives have made a presence in biomaterial science due to beneficial properties including non- toxicity, biodegradability, and biocompatibility. Cellulose derivatives (see **Figure 1** for the organic structures) have made a presence in biomaterial science due to beneficial properties including non-toxicity, biodegradability, and biocompatibility. EC exhibits excellent film-forming capacity, structural stability, and controlled drug release properties, making it highly effective for sustained therapeutic delivery. Its ability to be electrospun into fibrous matrices further enhances drug permeation and bioavailability, supporting its application in transdermal and biomedical platforms.[21] Additionally, EC has been successfully blended with other polymers, such as polyhydroxybutyrate, to enhance mechanical properties and control drug release kinetics, demonstrating its adaptability in composite formulations. These properties make EC-based scaffolds particularly useful for antibiotic and pharmaceutical delivery, with electrospun fibres

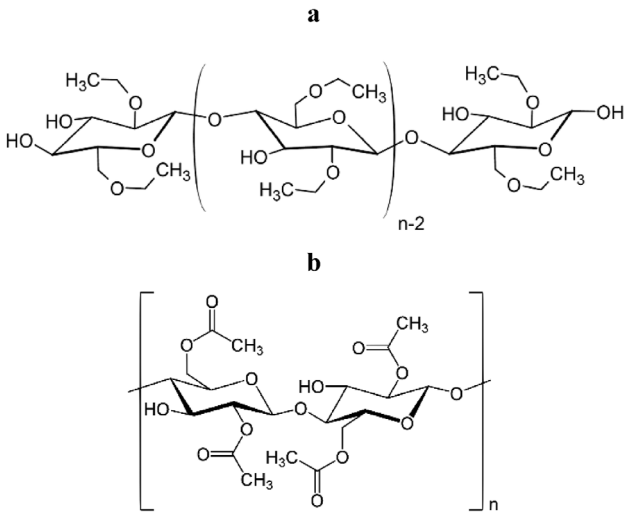

Figure 1. Structural representation of cellulose derivatives used in this study. The structures between EC a) and CA b) influence fibre morphology, drug encapsulation, and release behaviour, as explored in later analyses.

showing prolonged, controlled release patterns ideal for localised and sustained treatment.[22] CA is a widely used biomaterial in drug delivery systems due to its biocompatibility, biodegradability, and mechanical strength. Its versatility is further enhanced when blended with other polymers, such as polycaprolactone, to create fibre coatings on medical implants, offering tailored drug release patterns and improved mechanical attributes.[23] For example, a study developed an implantable drug delivery system using electrospun CA and PCL nanofiber membranes, achieving a prolonged and controlled release of the drug over an extended period.[24] The ability of cellulose derivatives to form binary systems with other polymers has been widely explored to enhance mechanical properties, drug release control, and biocompatibility. The structural advantages of binary polymeric systems have been applied across various biomedical fields, including bone tissue engineering, transdermal patches, and surgical sutures, highlighting their potential for use in this type of patch.[18–20] Polyvinylpyrrolidone (PVP) is also biocompatible and non-toxic, being successfully used across a variety of fibre applications.[25] Previous research has demonstrated the potential of incorporating PGS into fibres using polymers such as Zein and PVP, prompting further exploration of alternative polymer options to enhance the understanding in this field.[26,27] With its brilliant spinning properties, PVP and the cellulose derivatives have been combined to create patches. PVP was specifically chosen due to its proven role as a fibre-forming agent that enhances drug dispersion and stability, making it well-suited for controlled release formulations in transdermal applications.[28,29] Surfactants play a pivotal role in augmenting intralipid transport through multiple mechanisms, including increased permeability, altered lipid structures, reduced lipid resistance to the drug, minimized drug crystallinity, and the creation of a more humid environment conducive to drug delivery.[30,31] In this study, Polysorbate 80 (PS80), a surfactant widely used in the skincare industry for enhancing drug permeation through membranes, is employed to compare its effects on enhancing PGS through a commonly

Table 1. Polymer Solution compositions of 20 mL prior to electrospinning.

Reagents	EC			CA		
	-Blank	-Dry	-Wet	-Blank	-Dry	-Wet
PVP ($w_{pvp}/v_{solvent}$) %	16.25	16.25	16.25	16.25	16.25	16.25
Cellulose Derivative (w_{cd}/w_{pvp}) %	4.6	4.6	4.6	4.6	4.6	4.6
Total Polymer ($w_{polymer}/v_{solvent}$) %	17	17	17	17	17	17
PGS ($w_{PGS}/w_{totalpolymer}$) %	0	6	6	0	6	6
PS80 ($v_{ps80}/v_{solvent}$) %	0	0	5	0	0	5

used cellulose acetate membrane.[28,32,33] DMF and ethanol were used as solvents due to their effectiveness in dissolving cellulose acetate (CA) and ethyl cellulose (EC), respectively, for electrospinning. DMF ensures complete CA dissolution, while ethanol's faster evaporation aids in forming well-defined EC fibres.[34,35]

Electrospinning (ES) has been successful in fabricating fibres and scaffolds for various applications, including chemical, electrical, and medical. In ES, a polymer solution is injected through a metallic needle (positive electrode) connected to a high voltage ramp. The solution is spun onto a conductive collector plate (negative electrode) at a constant rate.[36] The difference in potential between the electrodes causes the solution to be drawn multiple times before reaching the collector plate. As the solution leaves the needle, it forms a Taylor cone due to electrostatic repulsion overcoming the fluid's surface tension. The emerging droplet changes from a circular shape to a conical Taylor cone. With increasing electric field strength, the polymeric jet stream passes through a stable zone, after which it experiences whipping and bending instabilities. The jet undergoes multiple draws before it begins to collect on the conductive plate, traversing through the air (resulting in solvent evaporation) and leaving behind fibres.[37] Factors such as solvent, solution viscosity, temperature, and relative humidity all influence fibre morphology.[26] This popular, intricate method of fibre fabrication is utilised to create binary-based transdermal patches for in vitro drug delivery. The in vitro transdermal study involves releasing PGS into non-toxic phosphate buffer saline (PBS) of 7.4 (commonly used across literature to simulate bodily fluids), with experiments shedding light on the effects of PS80 in PGS drug release into PBS. A supplementary drug release was done in PBS of pH level 6, to simulate skin acidity, which can be found in the Supporting Information.

This study pioneers the development of an electrospun fibrous matrix specifically designed for transdermal PGS delivery, a novel approach that has not been extensively explored in menopause management. Unlike conventional hormone delivery methods, this research introduces a binary polymeric system using EC and CA, optimised for controlled drug release and enhanced bioavailability. The incorporation of PS80 as a permeation enhancer is a key innovation, strategically improving drug absorption across the skin barrier—an aspect that has been underexplored in transdermal PGS formulations. Additionally, this study provides the first comparative analysis of EC and CA fibres for PGS delivery, offering critical insights into polymer selection for tailored drug release kinetics.[38] By addressing limitations such as hepatic metabolism, patient adherence, and inconsistent release rates in existing methods, this research lays a strong foundation for future in vivo investigations and potential clinical translation of electrospun fibrous patches as a next-generation hormone therapy for menopause.

2. Materials and Methods

2.1. Materials

PVP (Mw ≈ 1 600 000 g mol^{-1}), EC (455 g mol^{-1}), CA (264 g mol^{-1}), PGS (Mw ≈ 314 g mol^{-1}, aqueous solubility: 8.81 mg L^{-1} (at 25 °C), log P: 3.87), PS80, Phosphate Buffer Saline (PBS) pH = 7.4), Ethanol and Dimethylformamide (DMF) were obtained from Sigma-Aldrich, Dorset, UK. All were used without further purification. Ethanol and DMF were used as the solvent for this study. Cellulose acetate membranes of pore size 0.2 µm, obtained from Sartorius, Gottingen, Germany. were used for permeation studies.

2.2. Preparation of Polymer Solutions and Electrospinning

To study the effects of PS80 and PGS on cellulose derived nanofibres, six different polymer solutions tagged EC/CA-Blank, EC/CA-Dry, and EC/CA-Wet were created to perform two test sets, see **Table 1**. In the initial stages of our investigation, a thorough analysis of various electrospun fibre mats was conducted to identify the optimal fibres for our experiments. The selection criteria focused primarily on achieving the lowest standard deviation and the smallest fibre diameter. After careful evaluation, the fibre mats that best met these criteria were selected for subsequent experimental phases, see Supporting Information. The EC/CA-Blank solution was prepared with the use of a 4.6% w_{CD}/w_{PVP} EC/CA to PVP (16.25% $w_{PVP}/v_{Solvent}$ solution), resulting in a total 17% ($w_{Total\ Polymer}/v_{Solvent}$) of polymer to solvent solution. To prevent the evaporation of the volatile solvent during solution preparation, the cellulose derivative and PVP solutions in 20 mL capped glass vials were mixed, heated to 60 °C, and stirred for 30 h. After the polymers had completely dissolved, the solutions were cooled to 22 °C. The EC/CA-Dry solution was prepared with the same procedure as EC/CA-Blank but with an additional 200 mg of PGS. The EC/CA-Wet solution was prepared with the same procedure as EC/CA-Dry but with an additional 1 mL of PS80. The EC/CA-Blank solution was used as a control for FTIR and Rheology, and the EC/CA-Dry solution was used as a control within the test set for drug release.

A 10 mL syringe was filled with 5 mL polymer solution and connected to an orifice through a solution pipe. The syringe was inserted into a syringe pump, and the flow rate was set to 10 µL min^{-1}. The orifice was connected to a voltage supply through a positively charged electrode (anode) at a voltage of 10 kV, allowing a 15 cm gap between the positively charged orifice and the grounded collection plate. The spinning process was conducted at an ambient temperature of 22 °C at 40% relative humidity for 20 min, and the fibre sample was collected. A similar procedure was used in spinning EC/CA-Blank, EC/CA-Dry, and EC/CA-Wet fibres.

2.3. Rheology

Rotational rheological tests (cone-plane method) and the Du Noüy ring method were used to measure the viscosity and surface tension of the polymer solutions for insights into the rheological behaviour of the EC-PVP and CA-PVP solutions with EC/CA-Blank, EC/CA-Dry, and EC/CA-Wet configurations.[39,40] Mean surface tension values were calculated by taking three measurements from each solution.

2.4. Scanning Electron Microscopy

EC/CA-Blank, EC/CA-Dry, and EC/CA-Wet fibres were collected on carbon taped SEM studs to prepare for imaging. Scanning electron microscopy (Hitachi S-3400n) was used to examine the gold sputtered fibres at an accelerating voltage of 3 kV. ImageJ was used to measure the diameters of the fibres. Python and OriginPro were used to analyse the data and produce a distribution plot of the various fibre diameters. The experimental control for drug release was the dry fibres.[41,42]

2.5. Fourier Transform Infrared Radiation Spectroscopy

The interaction between the drug, polymers, and chemical reaction within the processed fibres was analysed using FTIR spectroscopy (PerkinElmer Spectrum 100). Prior to analysis, 2 mg of each sample (EC/CA-Blank, EC/CA-Dry, and EC/CA-Wet) was placed on the ATR crystal and studied over 10 rounds in the range of 500–4000 cm^{-1} at a resolution of 4 cm^{-1}.[42]

2.6. Drug Release and Mathematical Modelling

2.6.1. Drug Loading and Release

The solvent for the EC fibres was ethanol. The solvent for the CA fibres was DMF. For this study, drug release characteristics were analysed spectrophotometrically at 270 nm using a Jenway 6305 UV/Visible spectrophotometer (Bibby Scientific, Staffordshire, UK)[43,44] PS80 (Sigma–Aldrich, Dorset, UK) exhibits significant absorption at 234 nm, followed by a substantial decrease in absorption.[45,46] To investigate the drug's release dynamics from the polymer, comparative absorbance was used to analyse the movement of the drug into a fixed Franz Diffusion Cell volume of 5 mL.[15,27] This approach ensured that the drug consistently approached its maximum saturation point, providing insights into drug release within a controlled space and enhancing our understanding of polymer-drug interactions. Maintaining saturation within this consistent volume allowed for direct comparisons between different formulations, highlighting their distinct performance characteristics. Two main parts were conducted, focusing on the calculation of the actual drug content in the patches and the assessment of drug release. A reference blank sample of 11.2 mg fibres with no drug was measured using a UV machine at 270 nm, which was used to calibrate the machine when comparing to a loaded sample and was therefore the baseline for calibration and background correction. A test sample containing 11.9 mg fibres (either EC/CA-Dry or EC/CA-Wet) with the drug was compared against these blank fibres to account for a 6% increase in overall polymer weight due to PGS addition. This was consistent throughout the entire drug release study. For the first part, a calibration curve was generated to determine the concentration of PGS in ethanol and PGS in DMF. The calibration curve was used to calculate the drug content in the EC/CA-Dry and EC/CA-Wet fibre patches that were being tested. The encapsulation efficiency was also calculated by dividing the actual amount by the theoretical amount. In the second part, the comparative absorbance method was employed to record the drug release behaviour. Four additional calibration curves for EC/CA-Dry and EC/CA-Wet were established to determine the relationship between PGS content and patch weight in PBS. From the PBS based calibration curves, the maximum absorbance values for EC/CA-Dry and EC/CA-Wet were determined. These samples were fully submerged in PBS (receptor volume 5 mL), stirred magnetically for 24 h to achieve maximum internal drug release, and the absorbance at this stage was recorded as the final reference point. The drug release was finally conducted, whereby 11.9 mg of PGS loaded patches were placed on top of cellulose acetate membranes, releasing into a Franz Diffusion Cell (reception volume 5 mL). A reading was taken at time points, and after each reading, the samples were returned to the cells for subsequent measurements. Differences in drug release were recorded at various time points until reaching the maximum absorbance determined earlier. The top of the diffusion cell orifice with a 25.4 mm outer diameter was covered with parafilm and pierced to increase pressure in the fibre system. The cell was kept under a constant temperature of 35 °C to simulate skin temperature,[47,48] with a magnetic stirrer in the bath for adequate mixing of PGS transported through one membrane into the buffer solution of the accepting chamber. All tests were repeated three times each for accuracy.

2.6.2. Mathematical Modelling

Six different models described in **Table 2** were used to compare the experimental drug release to predictive kinetic and geometric models. DDSolver was used for kinetic models, and MATLAB was used for the geometric equation.[49]

3. Results

3.1. Rheology

The rheological properties for all solutions are shown in **Table 3**. When 0.2 g PGS was introduced into the polymer solution, both EC and CA solutions experienced a small decrease in viscosity, with values of 1.6% and 3.4%, respectively. However, the viscosity changes when adding PS80 were significantly different between the two cellulose forms. In the EC solution, viscosity increased by 10% between EC-Dry and EC-Wet, while in the CA solution, there was only a 0.3% increase. This difference can be attributed to two factors. First, CA has a lighter molecular weight compared to EC. Second, the choice of solvent affects viscosity, with ethanol being more viscous than DMF. When PGS was added, both solutions had a reduction in viscosity. This is because hydrophobic

Table 2. Mathematical Models.

Model	Equation	Parameters
First Order	$F = 100[1 - e\ (-k_1 t)]$	k_1 is the release rate constant, t is time.
Higuchi	$F = k_H t^{0.5}$	k_H is the release rate constant, t is time.
Weibull	$F = 100(1 - e^{-\frac{(t-T_i)^\beta}{\alpha}})$	α is the time process, T_i is the time lag, β is the shape parameter. β characterizes the curve as exponential ($\beta = 1$), S-shaped with an upward curve followed by a turning point ($\beta > 1$), or parabolic with higher h higher initial slope, after that consistent with the exponential ($\beta < 1$).
Makoid Banakar	$F = k_{MB} t^n e^{-kt}$	k_{MB} = release rate constant, n and k are empirical factors where k > 0.
Peppas Sahlin	$F = k_1 t^m + k_2 t^{(2m)}$	k_1 = constant related to the fickian kinetics, k_1 = the constant related to case- 2 relaxation kinetics, m is the diffusional exponent for a device of any geometric shape which inhibits controlled release.
Geometric Model	$Q = \frac{\beta(Dt)^{1/2}}{a}$	$\beta = 3.345$, D = diffusion constant, t = time, a = radius of fibres.

drugs can disrupt the arrangement of the polymeric chains, leading to reduced viscosity.[50] PS80 is a surfactant that affects the intermolecular forces between the polymer molecules and the solvent. The results suggest that PS80 has a stronger affinity for the functional groups of EC, leading to an 11% increase compared to a 0.3% increase in the CA solutions. For example, both EC and CA have hydroxyl (-OH) functional groups that can form hydrogen bonds with the hydrophilic polar head groups of PS80. EC's higher molecular weight, potentially attributed to its extensive ethoxylation of cellulose units, appears to be a leading factor distinguishing it from CA.[51,52] The results also showed that while the EC solutions had higher viscosity, their surface tension was lower. This is due to the use of ethanol as a solvent, which has a smaller molecular size and lower molecular weight compared to DMF. As a result, ethanol can more easily penetrate the surface layer of a liquid, causing a greater reduction in surface tension. The surface tension at room temperature for ethanol alone is 22.39 mN m^{-1}, while for DMF it is 37.1 mN m^{-1}.[53] Adding PS80 to both solutions reduced the surface tension, which is expected as surfactants adsorb at the air/solution interface when dissolved in water, leading to a decrease in surface tension.[54] Whilst the current data establishes the connection between viscosity and surface tension in fibre preparation, there is naturally scope for further exploration in future work. Future studies could investigate the impact of temperature variations on the rheological properties of these polymer solutions, particularly in relation to large-scale manufacturing and storage stability. Examining how temperature fluctuations influence viscosity, elasticity, and phase behaviour could provide additional insights for optimising processing conditions and ensuring reproducibility in industrial-scale fibre production.

3.2. Scanning Electron Microscopy

The morphological structures and diameters of EC and CA fibres are presented in **Figure 2** and **Table 4**. Electrospun fibres for drug delivery commonly range from 20 nm to 5 µm, with sizes tailored based on drug type, release kinetics, and application.[55] Drug-loaded fibres fall range and commonly fall between the 200 nm to 3 µm range to balance encapsulation efficiency and diffusion control.[56] To align with these established parameters, we designed our fibres within this range, with EC fibres (1.5–2.9 µm) and CA fibres (0.5–0.7 µm), ensuring consistency with controlled transdermal PGS release. The average diameter of EC-Blank fibres was measured to be 1.5 µm. Upon addition of PGS, the diameter increased by 13% to 1.7 µm, and with the addition of PS80, the diameter distribution rose by 33% to 2.9 µm. As for CA-Blank fibres, their average diameter was 0.5 µm. While the diameter remained unchanged after the addition of PGS, it increased by 40% to 0.7 µm with the addition of PS80. The EC fibres were ≈3 times larger than the CA fibres. This may be due to the increased molecular weight and more hydrophobic nature of the EC. Second, ethanol evaporates faster than DMF, which may also be a contributing factor to the increase in fibre diameter, as the more volatile a solvent, the greater the influence in diameter increases.[57,58] The encapsulation efficiency (EE) for EC-Dry and EC-Wet was 97% and 74%, respectively. For CA-Dry and CA-Wet, the EE is 89% and 80%, respectively.

3.3. Fourier Transform Infrared Spectrum

Figure 3 shows the results of the FTIR for both cellulose binary polymeric patches. Both EC/CA fibres exhibit a peak at

Table 3. Rheology of Solutions.

Polymer Solution	EC		CA	
	Viscosity [cP]	Surface Tension [mN m^{-1}]	Viscosity [cP]	Surface Tension [mN m^{-1}]
Blank	414.3 ± 1.3	28.3 ± 0.4	153.8 ± 0.3	39.8 ± 0.3
Dry	407.5 ± 0.7	26.3 ± 0.4	148.0 ± 0.3	40.5 ± 0.7
Wet	450.4 ± 1.3	25.7 ± 0.3	148.5 ± 0.5	34.1 ± 0.3

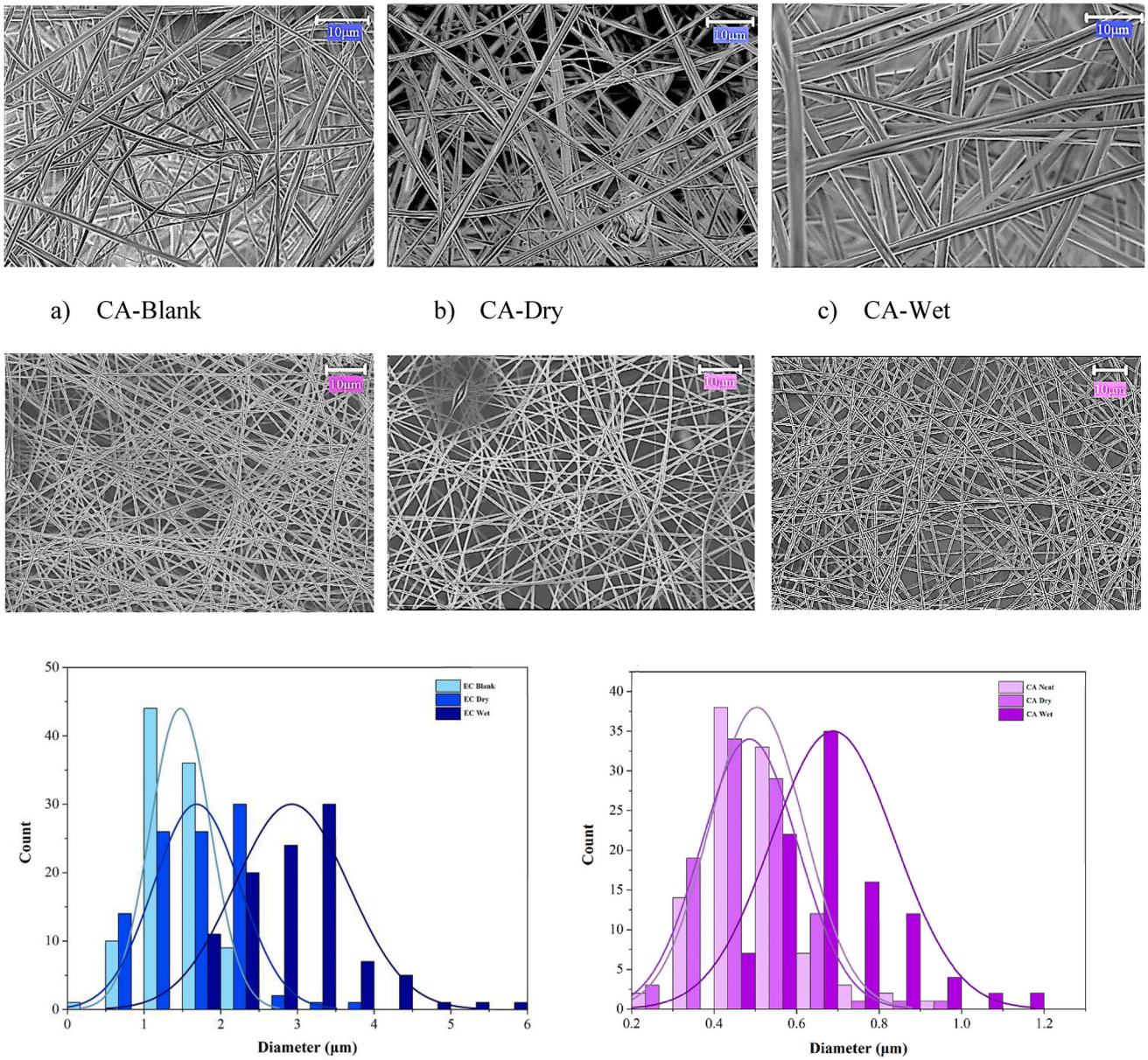

Figure 2. SEM Images of Cellulose -PVP fibres with respective diameter distributions with 10um scalebar. n = 100 for each sample.

1300 $cm^{-1,}$ indicating the presence of C-N resulting from the bonding between the carbon chain and ring structure of PVP. In addition, a peak at 1450 cm^{-1} is attributed to the bending vibrations of CH2 bonds in the carbon chain of the PVP monomers. The sharp maximum peak at 1650 cm^{-1} is associated with the stretching vibration of C═O stretching bonds in the carbonyl group of the PVP.[59] Stretching bands at 2800–3100 cm^{-1} confirm the presence of unsubstituted O—H bonds in the EC and CA monomers. The asymmetric C-H stretching in the EC monomer is represented by a broad peak at 3200–3600 cm^{-1}, while the final broad peak at 3200–3500 cm^{-1} shows the C-H bond in CA.[59–61] An additional weak peak at 2450 cm^{-1} is observed due to the bond interactions between PGS, EC, and PVP. The presence of PGS causes an overall absorbance drop of ≈10% in EC-Blank to EC-Dry, while the absorbance drop is ≈50% from CA-Blank to Dry. The absorbance drop in CA fibres is more pronounced than in EC, which may be attributed to the homogeneity of PGS across the fibres, as the standard deviation for the CA fibres is smaller than the EC fibres across all cases, as well as encapsulation due to evaporation when the polymer solutions were heated. The FTIR

Table 4. Results for Diameters.

Derivative	Blank	Dry	Wet
EC	1.5 μm ± 0.4	1.7 μm ± 0.6	2.9 μm ± 0.7
CA	0.5 μm ± 0.1	0.5 μm ± 0.1	0.7 μm ± 0.2

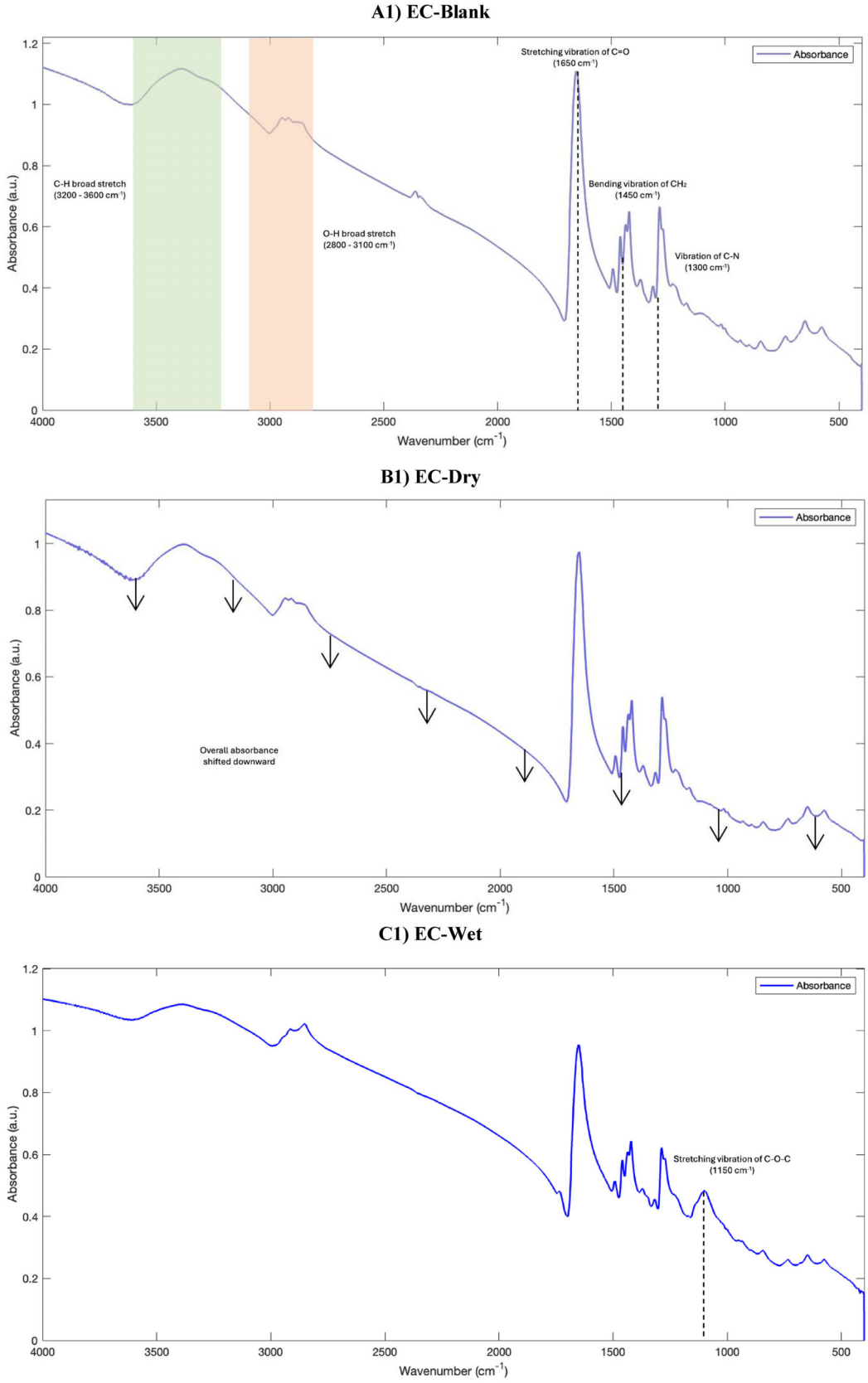

Figure 3. FTIR Absorbance Results Cellulose Derivative Fibres.

analysis confirmed the inclusion of PGS in fibres and provided further insight into the chemical composition and interaction of the various components in the fibres.[62–64]

Furthermore, an additional peak at 1150 cm^{-1} in both EC-Wet and CA-Wet is attributed to the C—O—C stretching vibration in the polyoxyethylene groups of PS80.[65] By introducing PS80, additional peaks were identified at 1150 and 2900 cm^{-1} that arise from the C—O—C stretching vibration in the polyoxyethylene groups and C—H stretching vibrations of methylene groups in the fatty acid esters of PS80 respectively.[65] PS80, which is an amphiphilic molecule, forms a micelle-like encasement that encloses PGS in a hydrophobic environment whilst facing the aqueous environment with its water-soluble hydroxyl and ether groups.[43] This encasement embeds the PGS into the EC and CA, ultimately enhancing the encapsulation efficiency. The hydrophilic surface of the PS80 encasement promotes the release of encased PGS when the patches are in an aqueous environment, explaining the increase in drug release rate.[66] Overall, the FTIR analysis not only confirmed the drug encapsulation but also that there were no new peaks, such as amide or nitrite peaks, indicating there was no chemical degradation. The core absorption bands of PGS remained intact, suggesting the drug's structure was preserved, and the polymer matrix provided stability without immediate breakdown.

The addition of PGS increases transmittance across both EC and CA, indicating reduced infrared absorption and successful drug incorporation – See **Figure 4**. The most significant shifts occur at 1650 cm^{-1} (C═O stretching in PVP) and 2800–3100 cm^{-1} (O-H stretching in EC/CA), suggesting that PGS disrupts hydrogen bonding within the polymer matrices.[59,60] This effect is more pronounced in CA, where transmittance increases nearly twice as much as in EC, implying better dispersion of PGS. This greater transmittance shift in CA can be attributed to its well-documented ability to form miscible blends with hydrophobic drugs like PGS, leading to better drug dispersion within the polymer matrix. This uniform distribution alters the polymer's infrared absorption characteristics more significantly, increasing transmittance compared to EC.[67]

The addition of PS80 introduces two new peaks at 1150 and 2900 cm^{-1} in both ECWet and CAWet, which were absent in ECDry and CADry, confirming successful PS80 incorporation. The 1150 cm^{-1} peak corresponds to C-O-C stretching vibrations in the polyoxyethylene groups of PS80, while the 2900 cm^{-1} peak is associated with C-H stretching in the fatty acid ester groups.[65,68] These spectral changes suggest that PS80 integrates into the polymer matrix rather than remaining surface-.[43] Notably, the 1150 cm^{-1} peak is more intense in CAWet than ECWet, suggesting that PS80 interacts more effectively with CA, likely due to better polymer compatibility.[69] This may indicate that PS80 disperses more uniformly within CA, supporting a micelle-like encapsulation effect that could enhance drug entrapment and release efficiency.[43] Despite these spectral changes, no major structural shifts are observed in either EC or CA, confirming that PS80 integrates into the fibres without chemically altering the polymer matrices.[62–64]

Despite the incorporation of PS80, the core transmittance profiles of both EC and CA remain largely unchanged, with no major shifts in characteristic polymer peaks. This indicates that PS80 does not degrade or chemically alter the polymer matrices, confirming the structural stability of the electrospun fibres.[70] Furthermore, the lack of unexpected peaks, such as amide or nitrite groups, reinforces that the encapsulation process did not introduce unintended chemical modifications to the polymer-drug system.[62–64] This structural stability is crucial for maintaining the integrity of the polymer matrix, ensuring that drug release properties are governed primarily by diffusion and micelle-driven release mechanisms, rather than polymer degradation.[54,71]

3.4. Results for the In Vitro Drug Release

The drug release curves are shown in **Figure 5**. The calibration curves for this study are given in Figure S8 (Supporting Information). The drug loading in EC-Dry and EC-Wet fibres samples being tested (11.9mg) is 600 µg ± 0.001 and 540 µg ± 0.001, respectively. The drug loading in CA-Dry and CA-Wet fibres samples being tested (11.9 mg) is 640 µg ± 0.004 and 500 µg ± 0.004, respectively. Observed (EC/CA) Dry and Observed (EC/CA) Wet are the experimental drug release data from EC/CA-Dry and EC-CA-Wet drug release studies. When incorporating PS80 into the EC fibres, there was 98% drug release by the end of the study in comparison to 87% without. For the CA fibres, there was a 96% drug release with the PS80, compared to 82% without. For both systems, there was a statistically significant difference in drug release when incorporating the PS80 ($p < 0.05$). Previous studies have explored the role of PS80 in electrospun drug delivery systems, but with less pronounced effects. Kazsoki et al. investigated PS80's impact on electrospun nanofibres and observed that PS80 made fibres stiffer and less plastic, but did not significantly enhance drug release rates.[72] In contrast, our study demonstrates a measurable 16%–17% improvement in release efficiency, reinforcing the role of PS80 in modifying polymer interactions to optimise transdermal drug permeability.

There was no significant difference between EC-Dry and CA-Dry and EC-Wet and CA-Wet ($p > 0.05$). For both systems, the release suggests burst release within the first 10 min, reaching 33% and 40% for EC-Dry and EC-Wet, respectively. Similarly, reaching 37% and 42% respectively for CA-Dry and CA-Wet within the first 10 min. Previous studies have shown that drug-polymer compatibility is key to controlling burst release in electrospun fibres. Zeng et al. found that poorly compatible drugs migrate to the fibre surface, causing high burst release, as seen with doxorubicin hydrochloride (70% release within 60 min).[73] In contrast, our study achieves a controlled burst release of 33–42% within 10 min, followed by sustained release up to 70 min. This improvement is due to better drug-polymer integration, ensuring a more gradual and predictable release profile instead of excessive early loss. The initial burst release in our study can be attributed to the dominating PVP presence in the patch, which is hydrophilic and therefore dissolved upon touching the cellulose acetate membrane. The remaining drug was released at a more consistent rate from 10 to 60 min for both investigations until ≈70 min, where there was no more drug release into the PBS cells. This reduced release rate can be attributed to the hydrophobic component of the cellulose derivative.

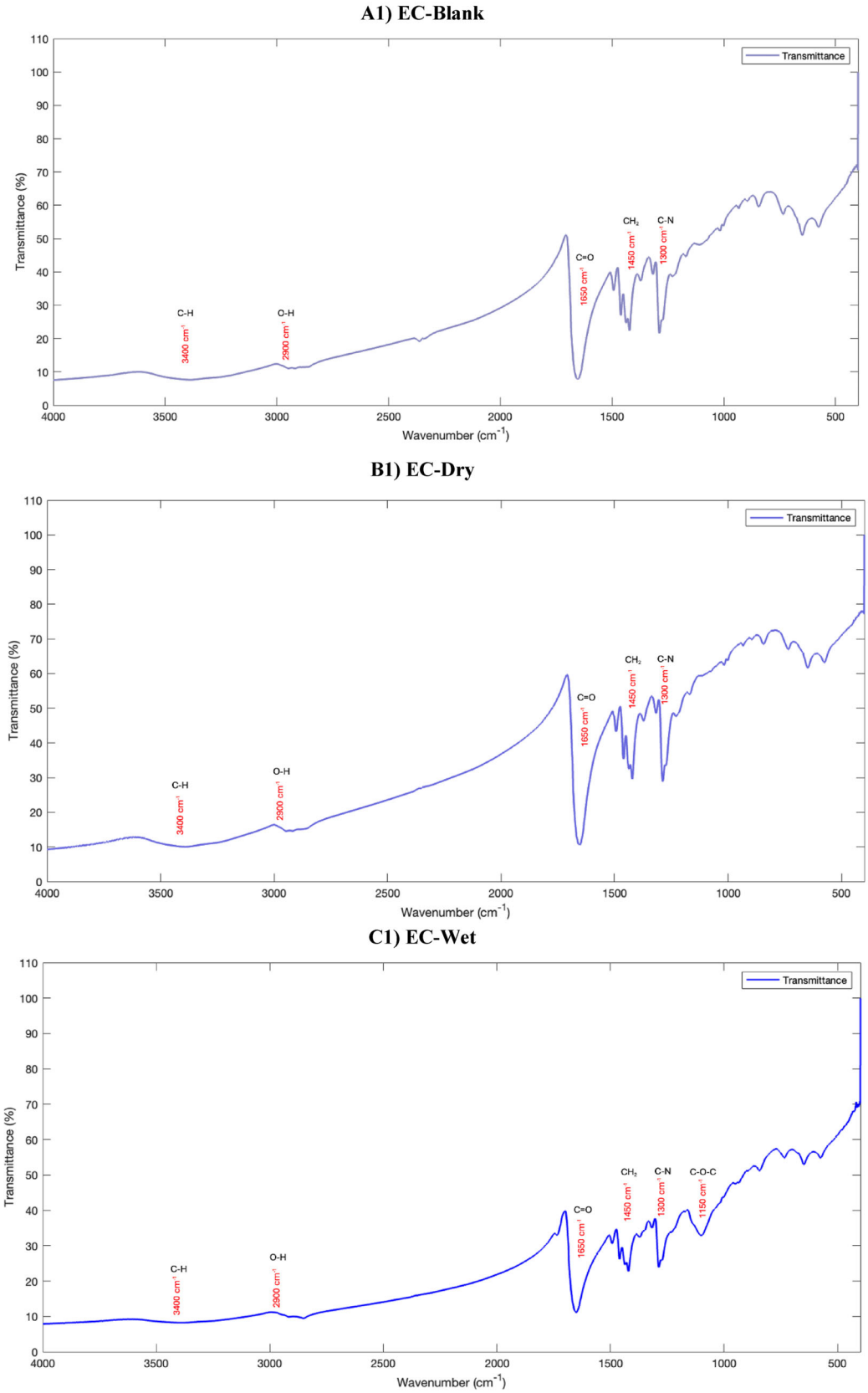

Figure 4. FTIR Transmission Results Cellulose Derivative Fibres.

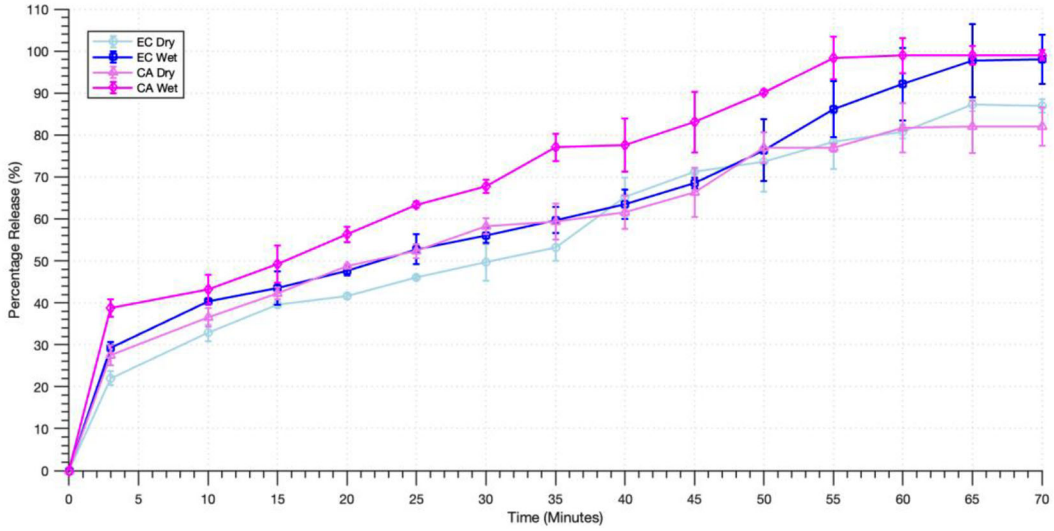

Figure 5. In Vitro Drug Release at pH 7.4. Error bars are present but too small to be visible due to minimal standard deviation (range: 0.001–0.024, detailed in the analysis). Significant differences in drug release between PS80-enhanced (EC-Wet, CA-Wet) and non-PS80 (EC-Dry, CA-Dry) formulations are marked with * ($p < 0.05$). No significant difference was observed between EC-Dry and CA-Dry or EC-Wet and CA-Wet ($p > 0.05$).

The study revealed that the EC-Wet/CA-Wet patch, weighing 11.9 mg, releases 540 µg/500 µg of PGS within 70 min into PBS through the Franz Diffusion Cell system. This result underscores the potential for future investigations. Notably, this release was observed in a PBS environment, providing a promising foundation for potential in vivo studies. For context, the Evorel patch (which is not solely progesterone) delivers 170 µg of PGS over 24 h.[74] The 60–70 min release window ensures a rapid progesterone dose reaches systemic circulation, complementing oestrogen therapy in hormone replacement. While oestrogel primarily alleviates acute menopausal symptoms, progesterone is essential for endometrial protection, especially when high-dose oestrogen is needed. Fast release provides immediate support for endometrial safety; however, this serves as a baseline demonstration of the patch's potential. With simple adjustments to its size and weight, clinicians can tailor the release profile to meet individual patient needs and clinical requirements, optimising long-term hormone delivery.[75] Research can further explore the tailored PGS delivery methods through the skin and assess their impact on the rate of drug release. Moreover, FTIR analysis indicated that the PGS fibre's crystalline structure may transition toward an amorphous state due to the surfactant, which could facilitate increased drug dissolution.

The surfactant's impact on lipid bilayers within the skin, promoting enhanced drug permeability, mirrors its effect on the cellulose acetate membrane, where it disrupts and modifies the organised polymer structure. This disruption relaxes the fibre network, increasing void spaces and enhancing overall porosity. By creating a more relaxed network with increased void spaces, PS80 further modifies fibre porosity, contributing to substructural changes that facilitate solvent penetration. Consequently, this structural change improves solvent penetration, facilitating greater interaction between water and the drug-loaded fibres, which accelerates dissolution and release.[43,44,76] Additionally, this substructural porosity enhances drug diffusion, ultimately improving permeability.[27] Furthermore, PS80 has an amphiphilic nature that allows it to form micelle-like structures, embedding PGS within the hydrophobic fibre core while maintaining a hydrophilic interface, promoting controlled drug release.[43] Together, these effects—improved fibre porosity and solubility—optimise drug permeability, supporting greater absorption in transdermal applications. These interactions provide valuable insights into the role of PS80 in ex vivo settings and, by extension, in vivo conditions.

The error bars were too small to be visually discernible on the graphs; therefore, for clarity, they were scaled by a factor of 200 in the figure. The actual standard deviations are as follows (to 3dp): for EC-Dry, the standard deviation values range from 0.001 to 0.009, and the average is 0.004. For EC-Wet, the standard deviation values range from 0.016 to 0.022, and the average is 0.018. For CA-Dry, the standard deviation values range from 0.008 to 0.015, and the average is 0.011. For CA-Wet, the standard deviation values range from 0.003 to 0.024, and the average is 0.014. The minor differences in drug release observed in the three sets of experiments can be ascribed to the limited drug volume employed. For both systems, adding PS80 to the system increased the standard deviation. This indicates a higher variability in the drug release data when PS80 was incorporated. The positive outcomes of this in vitro absorption study justify the need for further exploration through ex vivo and in vivo investigations. Such studies will provide a more comprehensive understanding of how the drug release profile translates to conditions closely resembling those in the human body. By addressing the observed variations across studies, a clearer picture of the drug's behaviour can be obtained, as seen in other studies.[77,78]

3.5. Mathematical Modelling

When comparing the observed drug release rates to the drug release models, it was evident that the magnitudes of the constants were higher for all wet models than for dry models (see

Table 5. Average RMSE and Parameters for EC Release Models.

Model	Average RMSE	Parameters for EC-Dry	Parameters for EC-Wet
First Order	5.3	$k_0 = 0.027$	$k_0 = 0.032$
Higuchi	3.7	$k_H = 10.2$	$k_H = 11.2$
Weibull	4.7	$\alpha = 92.6$ $\beta = 1.2$ Ti = −6.7	$\alpha = 8338.6$ $\beta = 2.2$ Ti = −30.6
Makoid Banakar	1.9	$k_{MB} = 14.638$ n = 0.385 k = −0.002	$k_{MB} = 18.231$ n = 0.363 k = −0.002
Peppas Sahlin	3.3	$k_1 = 8.6$ $k_2 = 1.3$ m = 0.4	$k_1 = 10.2$ $k_2 = 1.5$ m = 0.4
Geometric Model	7.8	$k_{Dry} = 1800$	$K_{Wet} = 7058$

Tables 5 and **6**. These increased drug release constants further confirmed the permeation enhancement of PS80. Upon investigation, the Makoid- Banakar model had the lowest RMSE of 1.9 for EC, while both the Makoid-Banakar and Peppas-Sahlin models had an RMSE of 2.4 for CA, indicating that these models best fit the drug release data for their respective polymer types. **Figures 6** and **7** visually demonstrate these fits, making it easier to assess release kinetics and trends beyond RMSE values alone, and **Figure 8** shows the optimal diffusion coefficient for use in geometric drug release modelling. A potential reason for the faster drug release rate in EC than CA may be attributed to the increased pore size that resulted from the higher diameter fibres.[79] Furthermore, as ethanol is more volatile than DMF and was used in EC, this may also be attributed to the larger pore size in the EC fibres, therefore allowing for easier diffusion of the drug out of the polymer matrix.[80,81] Beyond validation, modelling provides insight into whether diffusion or erosion, for example, governs release, aiding future patch optimisation and formulation predictability.

Table 6. Average RMSE and Parameters for CA Release Models.

Model	Average RMSE	Parameters for CA-Dry	Parameters for CA-Wet
First Order	4.5	$k_0 = 0.029$	$k_0 = 0.042$
Higuchi	2.5	$k_H = 10.293$	$k_H = 12.201$
Weibull	3.5	$\alpha = 11.824$ $\beta = 0.696$ Ti = −0.015	$\alpha = 15.892$ $\beta = 0.872$ Ti = −0.774
Makoid Banakar	2.4	$k_{MB} = 18.5$ n = 0.3 k = −0.004	$k_{MB} = 24.5$ n = 0.3 k = −0.005
Peppas Sahlin	2.4	$k_1 = 12.172$ $k_2 = 2.206$ $m = 0.327$	$k_1 = 14.038$ $k_2 = 2.971$ m = 0.32
Geometric Model	5.2	$k_{DRY} = 161$	$K_{Wet} = 547$

4. Conclusion

From the study, it can be concluded that electrospun PGS patches using EC or CA, combined with PVP, offer a promising alternative to traditional delivery methods. The addition of PS80 to both EC and CA fibres was assessed and found to increase the viscosity of the EC solution but not significantly affect the viscosity of the CA solution. The SEM results showed that EC fibres were thicker in diameter than CA fibres, for both dry and wet fibres. The FTIR results show that the absorbance drop is higher in the CA fibres. This may possibly be due to the increased homogeneity of PGS and encapsulation of the drug in the fibres.[62–64] Regarding the in vitro drug release rate, EC fibres had a higher release rate over the study than CA fibres for both dry and wet cases. Mathematical models, seen in Figures 6 and 7, were also used to analyse the data, and the Makoid Banakar model had the lowest average RMSE for EC, while both the Makoid-Banakar and Peppas-Sahlin model had the lowest average RMSE for CA.[79]

This study confirms the potential of electrospun PGS patches as a viable and effective transdermal drug delivery method, demonstrating successful drug permeation through a cellulose acetate membrane. By establishing the feasibility of electrospun fibres as a structured platform, this research validates key material properties and drug release characteristics, providing a solid foundation upon which future advancements can be built. The findings of this study demonstrate sufficient evidence to support further refinements while confirming the scientific and practical basis for the continued development of this system. Building on these foundations, the next steps should focus on refining structural characterisation, thermal properties, and biological evaluation. For example, while SEM provided sufficient resolution for fibre characterisation within the scope of this work, future refinements could incorporate TEM for higher-resolution imaging and a deeper understanding of fibre ultrastructure. Additionally, thermal stability has been effectively investigated at this stage, but further work could include melting point analysis via DSC to provide insight into phase transitions and material behaviour.

Beyond material properties, this study has effectively characterised drug release behaviour, confirming key kinetic trends and mechanisms. Future work may expand on this by integrating in vivo and ex vivo studies on biologically relevant skin models to further assess drug permeation, cytotoxicity, and overall biocompatibility. However, the current findings provide a clear mechanistic understanding of drug diffusion dynamics, forming a strong knowledge base for translation into biological models. Additionally, drug release from electrospun fibres is governed by diffusion dynamics, polymer-drug interactions, and fibre morphology, so a constant release rate is not typically expected. The observed variations align with biphasic behaviour, where an initial burst phase transitions into sustained release. While the current in vitro model effectively characterises drug release kinetics, in vivo studies and skin-mimicking models are beyond the scope of this work but have been identified as key future directions to further assess long-term stability, therapeutic effectiveness, and safety in biological environments. These findings collectively establish a strong scientific and practical foundation for the continued development of electrospun PGS patches as a viable transdermal drug delivery system. This study has successfully demonstrated material feasibility, drug release kinetics, and

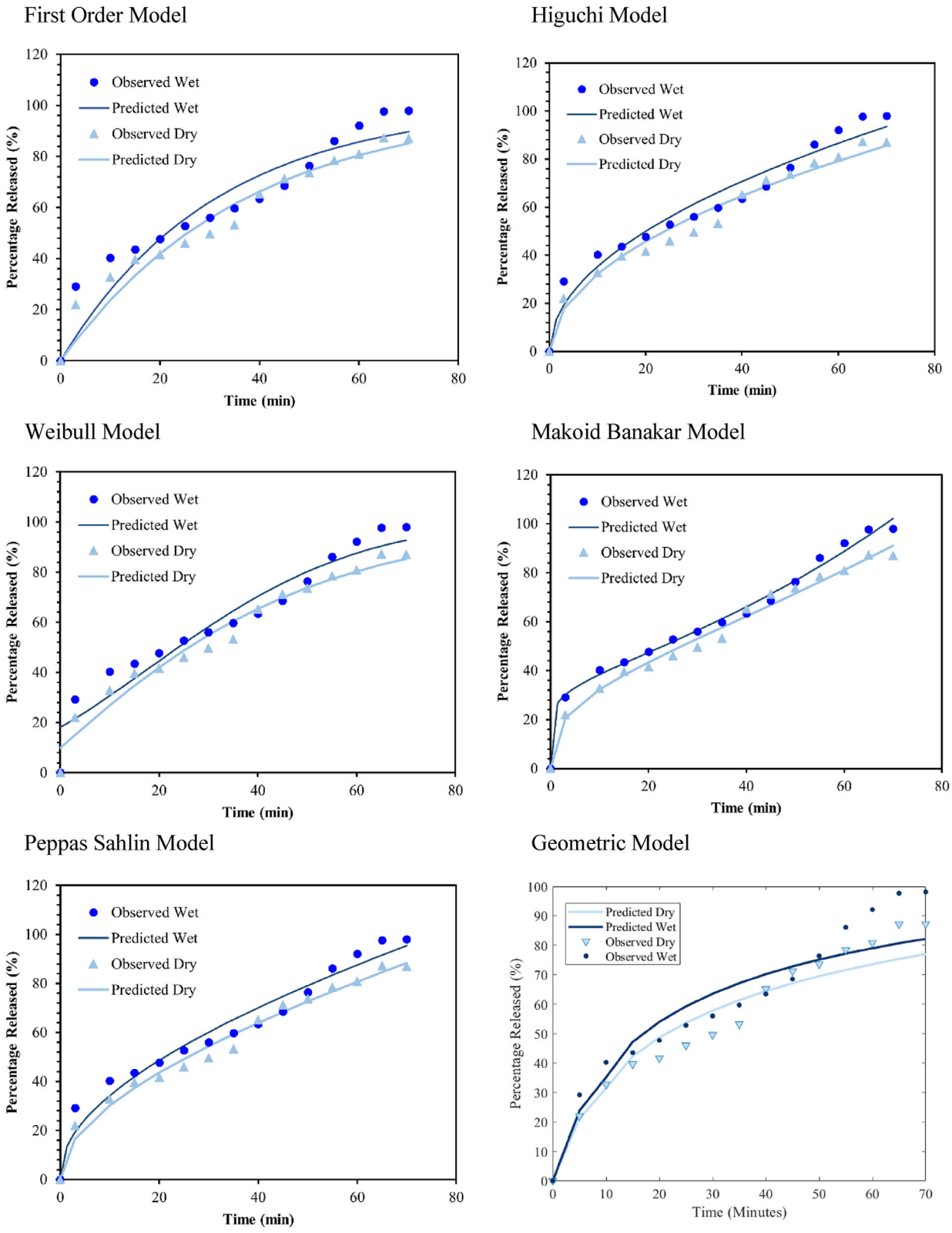

Figure 6. Experimental and Drug Release Models for EC Fibres.

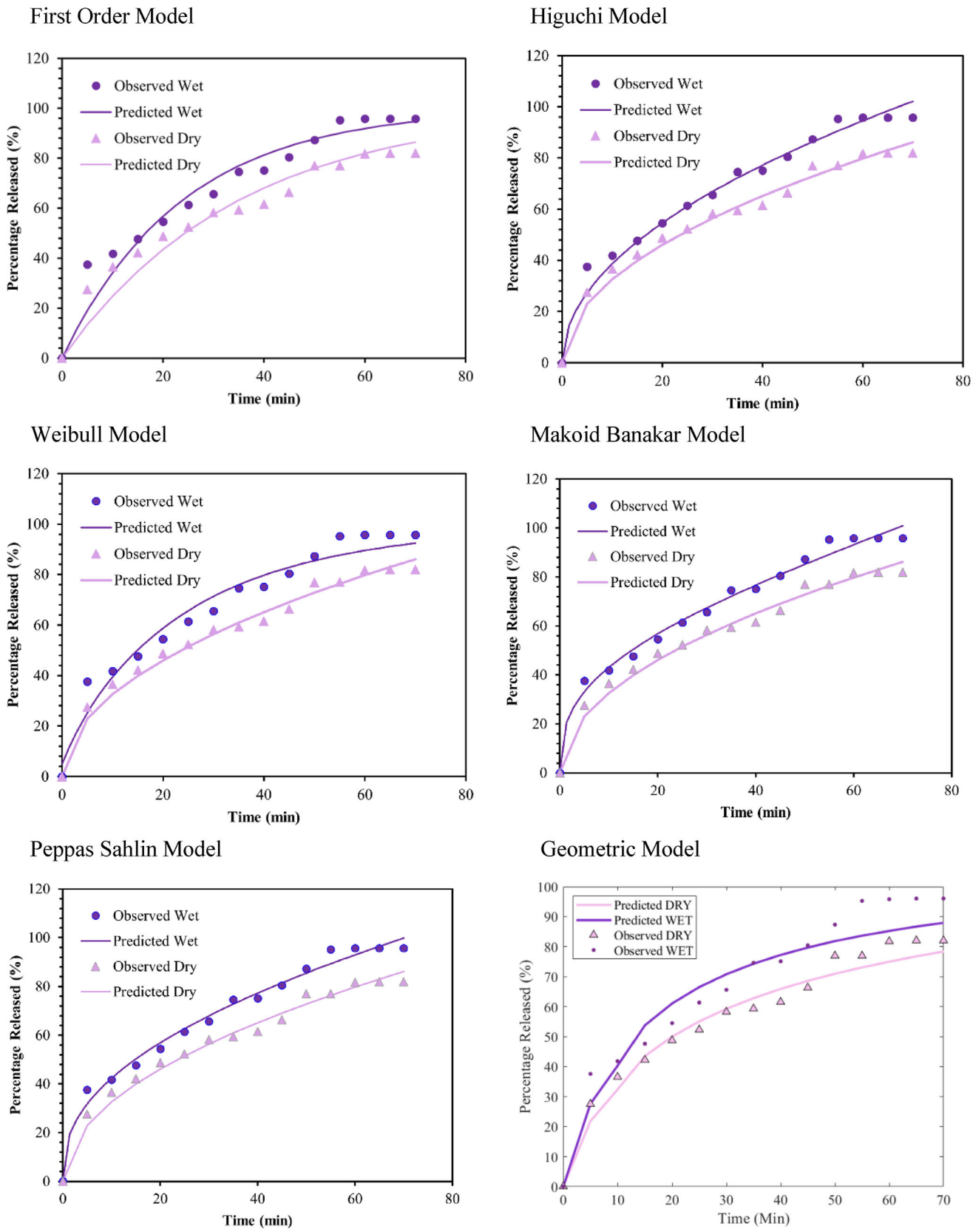

Figure 7. Experimental and Drug Release Models for CA Fibres.

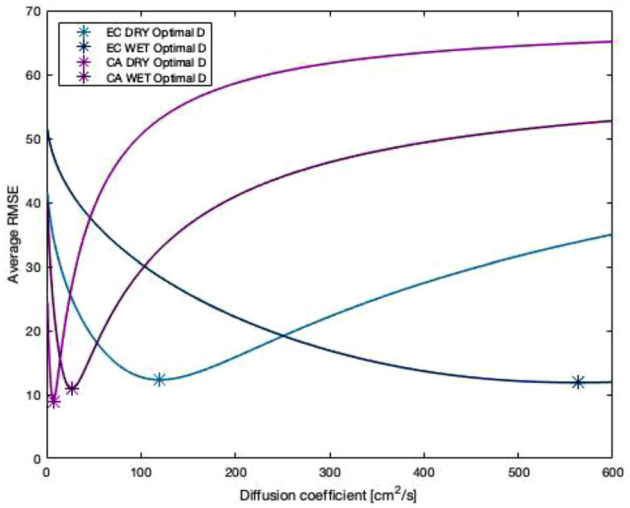

Figure 8. MATLAB Diffusion Coefficient Optimisation for use in the Geometric Model.

key formulation characteristics, providing the necessary groundwork for future optimisations. While further refinement and biological evaluations will strengthen clinical translation, the core advancements achieved here confirm that this fibre-based progesterone patch is ready for progression towards broader pharmaceutical and biomedical applications.

Supporting Information

Supporting Information is available from the Wiley Online Library or from the author.

Acknowledgements

Omar Shafi (OS) would like to thank the Sir Richard Stapley Educational Trust and UCL Mechanical Engineering for the financial and academic support throughout his PhD studies. Also, OS wishes to thank London Gynaecology for access to the clinical environment and expertise to supplement the research experience.

Conflict of Interest

The authors declare no conflict of interest.

Author Contributions

Dr. Omar Shafi, PhD, and a medical student, led the research, performed visualisation, characterisation, analysis, and wrote the initial draft. Ms. Michelle Swer, Consultant Obstetrician and Gynaecologist, along with Dr. Alisha Kassam, a Foundation Year 1 Doctor, and Mr. Mirkomol Mirzarakhimov, a medical student, managed the review of clinical literature. Engineering students Un Hou Chan and Jai Yi Huang assisted with experimental procedures and analysis. Dr. Francis Brako, Lecturer of Pharmacy, enhanced the analysis methods and contributed to both the pharmaceutical aspects and manuscript editing. Prof. Mohan Edirisinghe OBE refined the manuscript writing and provided overall supervision of the manuscript and research project. All authors contributed significantly to the research and approved the final manuscript.

Data Availability Statement

The data that support the findings of this study are available from the corresponding author upon reasonable request.

Keywords

biomaterials, cellulose acetate, electrospinning, ethyl cellulose, menopause, polysorbate, polyvinylpyrrolidone, progesterone, transdermal

Received: January 15, 2025
Revised: April 24, 2025
Published online: May 28, 2025

[1] R. A. Lobo, A. Gompel, *Lancet. Diabetes Endocrinol.* **2022**, *10*, 457.
[2] J. C. Harper, S. Phillips, R. Biswakarma, E. Yasmin, E. Saridogan, S. Radhakrishnan, M. C Davies, V. Talaulikar, *Women's Health* **2022**, *18*, 1.
[3] N. Dintakurti, S. Kalyanasundaram, P. Jha, V. Talaulikar, *Post Reprod. Health* **2022**, *28*, 137.
[4] N. Santoro, C. N. Epperson, S. B. Mathews, *Endocrinol. Metab. Clin. North Am.* **2015**, *44*, 497.
[5] S. S. Faubion, C. L. Kuhle, L. T. Shuster, A. Rocca, *H. Clinic, M. Clinic, M. Clinic* **2016**, *18*, 483.
[6] C. Campagnoli, F. Clavel-Chapelon, R. Kaaks, C. Peris, F. Berrino, *J. Steroid Biochem. Mol. Biol.* **2005**, *96*, 95.
[7] S. N. Dolitsky, C. N. C. Mitchell, S. S. Stadler, J. H. Segars, *Menopause* **2021**, *28*, 217.
[8] A. H. Clayton, P. T. Ninan, *J. Clin. Psychiatry* **2010**, *12*, 26233.
[9] S. Malik, K. Krishnaprasad, *J. Clin. Diagnostic Res.* **2016**, *10*, QE01.
[10] J. C. Harper, S. Phillips, R. Biswakarma, E. Yasmin, E. Saridogan, S. Radhakrishnan, M. C Davies, V. Talaulikar, *Women's Health* **2022**, *18*, 86.
[11] O. Shafi, M. Edirisinghe, U. Edirisinghe, B. Francis, in *Advances in Health and Disease*, Nova Publishers, London, **2021**.
[12] P.-Y. Scarabin, *Climacteric* **2018**, *21*, 341.
[13] X. Duan, H. Chen, C. Guo, *J. Mater. Sci. Mater. Med.* **2022**, *33*, 78.
[14] N. Talebi, D. Lopes, J. Lopes, A. Macário-Soares, A. K. Dan, R. Ghanbari, K. H. Kahkesh, D. Peixoto, P. S. Giram, F. Raza, F. Veiga, E. Sharifi, H. Hamishehkar, A. C. Paiva-Santos, *Appl. Mater. Today* **2023**, *30*, 101726.
[15] O. Shafi, *Doctoral Thesis*, University College London, London, UK **2024**.
[16] G. Cevc, *Expert. Opin. Investig. Drugs* **1997**, *6*, 1887.
[17] M. R. Prausnitz, V. G. Bose, R. Langer, J. C. Weaver, *Proc. Nat. Acad. Sci.* **1993**, *90*, 10504.
[18] A. Afshar, M. Gultekinoglu, M. Edirisinghe, *Int. Mater. Rev.* **2023**, *68*, 184.
[19] N.-I. Farkas, L. Marincaș, L. Barbu-Tudoran, R. Barabás, G. L. Turdean, *J. Funct. Biomater.* **2023**, *14*, 331.
[20] E. J. Torres-Martinez, J. M. Cornejo Bravo, A. Serrano Medina, G. L. Pérez González, L. J. Villarreal Gómez, *Curr. Drug. Deliv.* **2018**, *15*, 1360.
[21] A.-M. Croitoru, M. Ayran, E. Altan, Y. Karacelebi, S. Ulag, A. Sahin, M. M. Guncu, B. Aksu, O. Gunduz, B.-M. Tihăuan, D. Ficai, A. Ficai, *Int. J. Biol. Macromol.* **2023**, *253*, 126996.
[22] H. Karabulut, D. Xu, Y. Ma, T. A. Tut, S. Ulag, O. Pinar, D. Kazan, M. M. Guncu, A. Sahin, H. Wei, J. Chen, O. Gunduz, *Int. J. Biol. Macromol.* **2024**, *269*, 131794.
[23] C. Cidade do Carmo, M. Brito, J. P. Oliveira, A. Marques, I. Ferreira, A. C. Baptista, *Polymers (Basel)* **2024**, *16*, 2006.

[24] M. Ahmad Wsoo, S. Izwan Abd Razak, S. Shahir, H. Ahmed Abdullah Al-Moalemi, M. Rafiq Abdul Kadir, N. Hasraf Mat Nayan, *Polym. Adv. Technol.* **2021**, *32*, 3664.
[25] M. P. R. Guambo, L. Spencer, N. S. Vispo, K. Vizuete, A. Debut, D. C. Whitehead, R. Santos-Oliveira, F. Alexis, *Polymers (Basel)* **2020**, *12*, 1.
[26] C. Karuppannan, M. Sivaraj, J. G. Kumar, R. Seerangan, S. Balasubramanian, D. R. Gopal, *Nanoscale Res. Lett.* **2017**, *12*, 4.
[27] O. Shafi, S. Phadnis, U. H. Chan, M. Edirisinghe, F. Brako, *Macromol. Mater. Eng.* **2024**, *309*, 1.
[28] S. Manna, D. Dhanalakshmi, M. Bhowmik, S. Jana, S. Jana, *Front Mater* **2022**, *9*, 835507.
[29] P. Franco, I. De Marco, *Polymers (Basel)* **2020**, *12*, 1114.
[30] M. Kurakula, G. S. N. K. Rao, *J. Drug. Deliv. Sci. Technol.* **2020**, *60*, 102046.
[31] O. Shafi, M. Edirisinghe, F. Brako, *J. Drug. Deliv. Sci. Technol.* **2022**, *13*, 104062.
[32] R. Neupane, S. H. S. Boddu, J. Renukuntla, R. J. Babu, A. K. Tiwari, *Pharmaceutics* **2020**, *12*, 152.
[33] CIR, *Safety Assessment of Polysorbates as Used in Cosmetics*, CIR, Washington, DC **2015**.
[34] Q. Hao, J. Schossig, A. Towolawi, K. Xu, E. Bayiha, M. Mohanakanthan, D. Savastano, D. Jayaraman, C. Zhang, P. Lu, *ACS Appl. Engin. Mater.* **2024**, *2*, 2454.
[35] J. Matulevičius, L. Kliučininkas, D. Martuzevičius, *Chemija* **2014**, *25*, 125.
[36] S. G. Er, M. Edirisinghe, T. A. Tabish, *Adv. Healthcare Mater.* **2023**, *12*, 2201523.
[37] J. Guerrero, J. Rivero, V. R. Gundabala, M. Perez-Saborid, A. Fernandez-Nieves, *Proc. Nat. Acad. Sci.* **2014**, *111*, 13763.
[38] M. Janmohammadi, Z. Nazemi, A. O. M. Salehi, A. Seyfoori, J. V. John, M. S. Nourbakhsh, M. Akbari, *Bioact Mater* **2023**, *20*, 137.
[39] B.-B. Lee, E.-S. Chan, P. Ravindra, T. A. Khan, *Polym. Bull.* **2012**, *69*, 471.
[40] M. Keentok, R. I. Tanner, *J Rheol (N Y N Y)* **1982**, *26*, 301.
[41] M. Heidari, K. N. Onwukamike, E. Grau, S. Grelier, H. Cramail, M. A. R. Meier, A. Greiner, *Cellulose* **2021**, *28*, 6869.
[42] H. Majd, A. Harker, M. Edirisinghe, M. Parhizkar, *J Drug Deliv. Sci. Technol.* **2022**, *72*, 103359.
[43] M. Yasir, I. Som, K. Bhatia, *J. Pharm. Bioallied. Sci.* **2012**, *4*, 2.
[44] F. Han, S. Li, R. Yin, H. Liu, L. Xu, *Colloids Surf. A Physicochem. Eng. Asp.* **2008**, *315*, 210.
[45] W. Peter Wuelfing, K. Kosuda, A. C. Templeton, A. Harman, M. D. Mowery, R. A. Reed, *J. Pharm. Biomed. Anal.* **2006**, *41*, 774.
[46] Y. Zhang, P. Qi, *J. Pharm. Sci. Biomed. Anal.* **2017**, *1*, 111.
[47] P. Mehnert, J. Malchaire, B. Kampmann, A. Piette, B. Griefahn, H. Gebhardt, *Eur. J. Appl. Physiol.* **2000**, *82*, 52.
[48] Y. Zhang, P. Qi, *Pharmaceutical Sci. Biomed. Analysis J.* **2017**, *1*, 111.
[49] Y. Zhang, M. Huo, J. Zhou, A. Zou, W. Li, C. Yao, S. Xie, *AAPS J.* **2010**, *12*, 263.
[50] A. Spernath, A. Aserin, *Adv. Colloid Interface Sci.* **2006**, *128–130*, 47.
[51] J. Bicerano, *Prediction of Polymer Properties*, CRC Press, Boca Raton, FL, **2002**.
[52] H. Sohi, Y. Sultana, R. K. Khar, *Drug Dev. Ind. Pharm.* **2004**, *30*, 429.
[53] W. M. Haynes, *CRC Handbook of Chemistry and Physics* (Ed.: W. M. Haynes), CRC Press, Boca Raton, FL **2014**.
[54] S. Kotta, A. W. Khan, K. Pramod, S. H. Ansari, R. K. Sharma, J. Ali, *Expert Opin. Drug Deliv.* **2012**, *9*, 585.
[55] N. Kalayil, A. A. Budar, R. K. Dave, *BIO Integration* **2024**, *5*, 978.
[56] S.-F. Chou, D. Carson, K. A. Woodrow, *J. Controlled Release* **2015**, *220*, 584.
[57] P. Nuamcharoen, T. Kobayashi, P. Potiyaraj, *Polym. Int.* **2021**, *70*, 1465.
[58] T. Vongsetskul, T. Chantarodsakun, P. Wongsomboon, R. Rangkupan, P. Tangboriboonrat, C. Mai, *J. Sci.* **2015**, *42*, 436.
[59] A. E. Deniz, H. A. Vural, B. OrtaÇ, T. Uyar, *Mater. Lett.* **2011**, *65*, 2941.
[60] E. Huda, K. Rahmi, *IOP Conf. Ser. Earth Environ. Sci* **2019**, *364*, 012021.
[61] D. M. Patel, R. H. Jani, C. N. Patel, *Int. J. Pharm. Investig.* **2011**, *1*, 172.
[62] M. U. Akram, M. Nesrullah, S. Afaq, W. M. A. Malik, A. Ghafoor, M. Ismail, H. Nawaz, M. Ibrahim, F. Verpoort, A. H. Chughtai, *New J. Chem.* **2024**, *48*, 11542.
[63] K. H. Lee, F. N. Khan, L. Cosby, G. Yang, J. O. Winter, *Front. Nanotechnol.* **2021**, *3*, 719710.
[64] S. Sunoqrot, A. Alsadi, O. Tarawneh, R. Hamed, *Colloid Polym. Sci.* **2017**, *295*, 2051.
[65] Sigma Aldrich IR Spectrom Table, Wiley Science Solutions https://sciencesolutions.wiley.com/solutions/technique/ir/sigma-aldrich-library-of-ft-ir-spectra/ (accessed: December 2024).
[66] V. Ravichandran, M. Lee, T. G. Nguyen Cao, M. S. Shim, *Appl. Sci.* **2021**, *11*, 9336.
[67] G. O. do Nascimento Soares, R. Ribeiro Lima Machado, M. Mendonça Diniz, A. B. da Silva, *Polym. Eng. Sci.* **2020**, *60*, 3231.
[68] Sigma Aldrich, TWEEN® 80 viscous liquid | 9005-65-6 | Sigma-Aldrich, https://www.sigmaaldrich.com/catalog/product/sial/p1754?lang=en&region=GB (accessed: November 2024)
[69] D. M. Da Costa, V. R. R. Cunha, G. F. Perotti, R. R. Henriques, J. Amim Júnior, A. L. Shiguihara, *Orbital: The Electron. J. Chem.* **2020**, *12*, 30.
[70] H. Cortés, H. Hernández-Parra, S. A. Bernal-Chávez, M. L. Del Prado-Audelo, I. H. Caballero-Florán, F. V. Borbolla-Jiménez, M. González-Torres, J. J. Magaña, G. Leyva-Gómez, *Materials* **2021**, *14*, 3197.
[71] I. Negut, B. Bita, *Pharmaceutics* **2023**, *15*, 976.
[72] A. Kazsoki, P. Szabó, A. Domján, A. Balázs, T. Bozó, M. Kellermayer, A. Farkas, D. Balogh-Weiser, B. Pinke, A. Darcsi, S. Béni, J. Madarász, L. Szente, R. Zelkó, *Mol. Pharm.* **2018**, *15*, 4214.
[73] J. Zeng, L. Yang, Q. Liang, X. Zhang, H. Guan, X. Xu, X. Chen, X. Jing, *J. Controlled Release* **2005**, *105*, 43.
[74] Evorel, Evorel® Conti 50/170 micrograms per 24 hours transdermal patch, https://www.hpra.ie/img/uploaded/swedocuments/2ac5997b-9f29-4182-8deb-aec4010bec83.pdf (accessed: November 2024)
[75] EMA, *Guideline on Quality of Transdermal Patches*, European Medicines Agency, London, **2014**.
[76] S. Bolandi, F. Z. Ashtiani, A. Okhovat, M. B. Ghandashtani, *Theor. Found. Chem. Eng.* **2020**, *54*, 931.
[77] E. Abd, S. A. Yousef, M. N. Pastore, K. Telaprolu, Y. H. Mohammed, S. Namjoshi, J. E. Grice, M. S. Roberts, *Clin. Pharmacol.* **2016**, *8*, 163.
[78] M. Teaima, R. Abdelmonem, Y. A. Adel, M. A. El-Nabarawi, T. M. El-Nawawy, *Drug Des. Devel. Ther.* **2021**, *15*, 4603.
[79] M. T. Nelson, J. P. Keith, B. B. Li, D. L. Stocum, J. Li, *Proc. Inst. Mech. Eng., Part N: J. Nanoengin. Nanosystems* **2012**, *226*, 111.
[80] Q. Wu, W. Xie, H. Wu, L. Wang, *RSC Adv.* **2019**, *9*, 34486.
[81] J. Yang, R. Pal, *Polymers (Basel)* **2020**, *12*, 2302.

